

Charge transfer in T/H heterostructures of transition metal dichalcogenides

Irián Sánchez-Ramírez,^{1,2} Maia G. Vergniory,^{1,3} and Fernando de Juan^{1,2,4}

¹*Donostia International Physics Center, P. Manuel de Lardizabal 4, 20018 Donostia-San Sebastian, Spain*

²*Departamento de Física de Materiales, Facultad de Ciencias Químicas, Universidad del País Vasco (UPV-EHU), P. Manuel de Lardizabal 3, 20018 Donostia-San Sebastian, Spain*

³*Max Planck Institute for Chemical Physics of Solids, 01187 Dresden, Germany*

⁴*IKERBASQUE, Basque Foundation for Science, Maria Diaz de Haro 3, 48013 Bilbao, Spain*

(Dated: June 26, 2024)

The $\sqrt{13} \times \sqrt{13}$ charge density wave state of the T polytype of MX_2 ($\text{M}=\text{Nb}, \text{Ta}$, $\text{X}=\text{S}, \text{Se}$) is known to host a half-filled flat band, which electronic correlations drive into a Mott insulating state. When T polytypes are coupled to strongly metallic H polytypes, such as in T/H bilayer heterostructures or the bulk 4H_b polytype, charge transfer can destabilize the Mott state, but quantifying its magnitude has been a source of controversy. In this work, we perform a systematic ab-initio study of charge transfer for all experimentally relevant T/H bilayers and bulk 4H_b structures. In all cases we find charge transfer from T to H layers which depends strongly on the interlayer distance but weakly on the Hubbard interaction. Additionally, Se compounds display smaller charge transfer than S compounds, and 4H_b bulk polytypes display more charge transfer than isolated bilayers. We rationalize these findings in terms of band structure properties, and argue they might explain differences between compounds observed experimentally. Our work reveals the tendency to Mott insulation and the origin of superconductivity may vary significantly across the family of T/H heterostructures.

I. INTRODUCTION

Metallic transition metal dichalcogenides (TMD) MX_2 ($\text{M}=\text{Nb}, \text{Ta}$, $\text{X}=\text{S}, \text{Se}$)¹⁻³ are layered compounds made by stacking two basic MX_2 monolayer units known as H, with trigonal prismatic coordination of the metal, and T, with octahedral coordination⁴. Despite both having partially filled metal d -orbital bands, the low temperature properties of these building blocks are markedly different: while H layers show weak charge density waves (CDW) and remain metallic and often superconducting², T layers are understood to be Mott insulators⁵. The reason for this is the strong Star of David (SoD) $\sqrt{13} \times \sqrt{13}$ CDW reconstruction⁶, which gaps out most of the Fermi surface, leaving a half-filled flat band at the Fermi level which derives from an isolated orbital located at the SoD centers. The presence of even moderate Coulomb repulsion in these orbitals should thus drive this system to a Mott insulator state⁵, and perhaps a spin liquid⁷. The realization of such states in the bulk 1T polytype, made of stacked T layers, is however complicated by interlayer tunneling and the many possible CDW stacking patterns⁸. However, the recent synthesis of T monolayers⁹ has provided stronger support to the Mott insulator scenario.

TMD heterostructures alternating T and H layers provide an interesting alternative to put the hypothesis of the Mott insulator to test. In these structures the SoD moments from the T layer are coupled to the metallic electrons from the H layer, providing a natural realization of a CDW-induced Kondo lattice. Recently synthesized T/H bilayers have indeed showed prominent zero bias peaks in TaSe_2 ^{9,10}, TaS_2 ^{11,12} and NbSe_2 ^{13,14} which have been interpreted as the Kondo effect. In addition to such isolated bilayers, two naturally occurring bulk poly-

types formed by alternating T and H layers also exist, known as 4H_b ^{15,16} (with an inversion symmetric stacking of T/H bilayers) and 6R ^{17,18} (with an inversion breaking rhombohedral stacking). Interest in such compounds has been recently renewed because, in addition to displaying similar Kondo effects^{19,20}, 4H_b - TaS_2 shows unexpected signatures of unconventional superconductivity²¹: spontaneous breaking of time-reversal symmetry at T_c ²², spontaneous vortices in the superconducting state²³, superconducting edge modes²⁴ and transport evidence of a two-component order parameter^{25,26}.

The interpretation of all of these experiments and the relevance of the Mott insulator picture is critically dependent on two properties of the T/H interface which have remained under certain controversy: the interlayer hybridization V and the charge transfer $\Delta C = (C_H - C_T)/2$. Indeed, the T layer can only remain a Mott insulator if the flat band is nearly half-filled, but since the work function of the H layer is larger than that of the T layer, some amount of charge transfer from T to H is expected²⁷⁻²⁹. The Kondo effect similarly can only survive a certain charge transfer, and in addition it is only realized for a critical hybridization $V > V_c$. Superconductivity is also expected to be very different depending on whether the T layer contributes magnetic moments or not. A recent work has advocated the picture of a doped Mott insulator with negligible V ³⁰. Importantly, the effect of interlayer charge transfer in bulk 4H_b compounds has not been addressed to date, nor the potential variability in the different members of the family, TaS_2 , TaSe_2 or NbSe_2 .

In this work, we conduct a systematic study of charge transfer across all these compounds, exploring its correlation with work function mismatch, Van der Waals corrections, Hubbard's U parameter and interlayer spacing.

Our calculations reveal that the influence of U and Van der Waals effects is minimal while we observe that charge transfer is inversely related to the distance between layers and directly linked to the mismatch in work functions. In addition, we find the general trend that Se compounds display smaller charge transfer than S compounds, and $4H_b$ bulk polytypes display more charge transfer than isolated bilayers.

II. CHARGE TRANSFER IN T/H STRUCTURES

Early works^{27–29} already anticipated that charge transfer from the T to the H layers must be present in bulk $4H_b$ TMDs. At high temperatures where the CDW in the T layers is incommensurate, the change in CDW wavevector compared to bulk 1T polytypes was used to estimate a transfer of $0.12 e^-$ per formula unit²⁷ ($1.56 e^-$ per SoD) in $4H_b$ -TaS₂, and a similar estimate leads to $1.20 e^-$ per SoD for TaSe₂. Similar theoretical estimates²⁹ for $4H_b$ -TaS₂ similarly ranged between 1.04 to $1.43 e^-$ per SoD. Charge transfer of this magnitude was also reported to be consistent with changes in the optical conductivity in both $4H_b$ and $6R$ polytypes²⁸. More recent ARPES experiments estimated $0.92 e^-$ per SoD in $4H_b$ -TaS₂³¹. All these early estimates are thus consistent with a nearly empty flat band.

Recent ab-initio calculations in the high temperature state without CDW^{32,33} also suggest charge transfer from T to H, but given the strong band reconstruction due to the CDW, it is important to perform these calculations in the CDW state. Such calculations^{20,24} for a T/H bilayer of TaS₂ still report a fully empty flat band, while a bilayer T on monolayer H reported $0.31 e^-$ per SoD cell³⁴. For TaSe₂, a value of $0.32 e^-$ per SoD cell was reported¹⁰, while for NbSe₂ $0.17 e^-$ was calculated³⁵. A recent study has emphasized the importance of the stacking distance on charge transfer³⁰, revealing that ΔC ranges from 0.4 to 1 in TaS₂ as the interlayer distance goes from 7 to 5.8 Å.

Given such variability, and the fact that isolated bilayers on substrates may not stack with the same interlayer distance as bulk $4H_b$ compounds, it is important to study the distance dependence in detail for TaSe₂ and NbSe₂. Differences may be expected because the flat band in the Se compounds is significantly closer to the CDW valence bands compared to the S compounds. For NbSe₂ one experiment has claimed¹⁴ a charge transfer with an opposite sign to that of the Ta compounds. It is also important to take into account the details of the different ab-initio calculations done for the T compounds^{36–42}, for example because the exact position of the flat band within the CDW gap is known to depend on the functional used⁴³, which can influence charge transfer. Including the Hubbard interaction and explicitly accounting for magnetic states with spin-split bands^{43–47} can similarly affect the charge transfer.

Finally, note in the context of correlated systems the term charge transfer is often used to emphasize the distinction between Mott and charge transfer insulators⁴⁸. In that case, the term refers to charge transfer between correlated d -derived bands and the dispersive p -derived bands of the same compound. In TMDs this phenomenon may also be relevant at least for some compounds like 1T-NbSe₂ or 1T-TaSe_xTe_{1-x} where the flat band may overlap with the p -derived states^{13,43,49}. In our work, unless specified otherwise, charge transfer will rather refer to interlayer charge transfer between the T and the H layers.

A. Ab-initio methods

The aim of this work is to provide a systematic study of the interlayer charge transfer between T and H MX₂ layers. The workflow used to carry out said study is as follows:

1. Single layer in-plane structure relaxation for H and T layers.
2. Single layer workfunction calculation for H and T layers.
3. T-H bilayer relaxation, first relaxing in the \hat{z} direction followed by a subsequent in-plane relaxation.
4. Charge transfer calculation for bilayers. In this step we explore different parameters as Hubbard U , Van der Waals corrections and inter-layer distance dependence.
5. $4H_b$ charge transfer calculation using step 2 structures and experimental distances.

The purpose of this workflow is to identify trends between different factors affecting *ab-initio* calculations and experimental measurements, aiming to understand the overall behaviour of charge transfer under different conditions. All calculations were performed using Vienna Ab initio Simulation Package (VASP)^{50,51} v.6.2.1. with projector-augmented wave pseudopotentials within the Perdew Burke Ernzerhof parametrization⁵². For step 1 and 3, the relaxation was conducted by using the conjugate-gradient algorithm as implemented in VASP, and setting the ionic positions as the sole degree of freedom. For steps 1 – 4, calculations were found to be well converged with a 480 eV kinetic cutoff and a gamma-centered $15 \times 15 \times 1 k$ -mesh. Meanwhile, for step 5, the self-consistent calculations were found to be well converged with a 480 eV kinetic cutoff and a gamma-centered $13 \times 13 \times 3 k$ -mesh. In step 4, when Van der Waals corrections were considered, DFT-D3 method⁵³ with zero damping was used. Also in step 4, in order to study the effect of Coulomb repulsion, the DFT+U rotationally invariant approach⁵⁴ was followed by setting different effective on-site U Coulomb interactions in M's

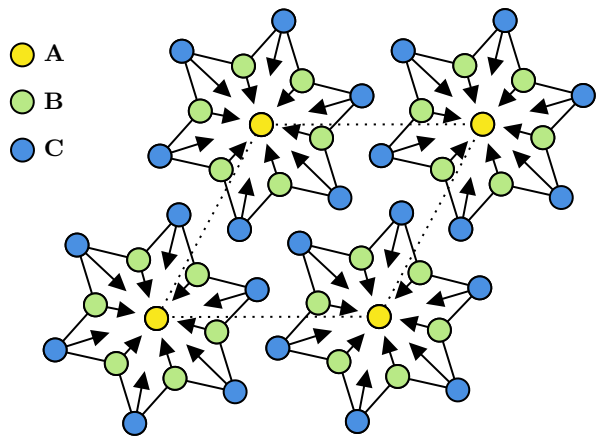


FIG. 1. Lattice structure of the SoD CDW distortion of the 1T polytypes. A, B, C inequivalent metal sites are marked in yellow, green and blue respectively. Black arrows show their displacements while a dotted line marks the CDW unit cell.

d -orbitals with $J = 0$. These DFT+U calculations are the only collinear spin-polarized ones. The initial magnetization was set to $1.4\mu_B$ for the central Ta/Nb atom (A atom, see Sec. II B), and zero for the remaining atoms. This choice is based on prior studies suggesting that the predominant magnetic moment is concentrated at the center of the SoD³⁸, and that the total magnetic moment is typically around $1\mu_B$ ^{44,46}. The initial value of magnetization is taken slightly larger than the expected result as this is expected to improve convergence⁵⁵. Atom-projected band structures were obtained using PyProcar⁵⁶ package for Python.

B. Charge density wave distortions

The $\sqrt{13} \times \sqrt{13}$ SoD CDW structure is shown in Fig. 1. There are three types of symmetry equivalent M sites labeled as A, B and C hereafter, with multiplicities 1, 6, and 6 respectively. The structure is parametrized by three independent displacements \vec{u}_i with $i = A, B, C$, shown in Fig. 1 ($|\vec{u}_A| = 0$ by symmetry). In table I we present the displacements for each equivalent metal site in each 1T-MX₂. In appendix A we present a graphic depiction of these displacements for the four compounds (Fig. 9) along a brief note on how we obtained the CDW positions.

C. Work function analysis

We define the work function as the absolute Fermi level with respect to vacuum. Different work functions between two structures indicate misaligned Fermi levels and can be used for a qualitative estimate of charge transfer. To compute the work functions, we perform a self-consistent calculation of the monolayer in a unit cell

with $\approx 20 \text{ \AA}$ of vacuum in the normal direction. From this calculation we extract the local potential $V(\vec{r})$ and define the work function as

$$W = V_{\text{vac}} - E_F, \quad (1)$$

where V_{vac} is the value of $V(\vec{r})$ in vacuum. We present the work functions for both T and H polytypes of all TMDs considered in table I. H work function is greater than T work function for all TMDs which anticipates that the charge transfer will occur from T to H layer. In Table I we can already see some trends: M=Ta compounds have overall smaller work function than M=Nb and so happens with X=Se when compared with X=S ones. In section II D we will see how this affect the charge transfer.

The work function results in Table I are consistent with Ref.³⁴, which reported work function values of $W = 5.35 \text{ eV}$ for T-TaS₂ in the CDW state, and $W = 6.07 \text{ eV}$ for H-TaS₂ in the 3×3 CDW state. Here we calculated $W = 5.19 \text{ eV}$ for T-TaS₂ in the CDW state, and $W = 5.57 \text{ eV}$ for 1H-TaS₂ without CDW. We opted not to include the 3×3 CDW state in H-TaS₂ layers in our calculations due to the excessive computational cost of a unit cell commensurate with both $\sqrt{13} \times \sqrt{13}$ and 3×3 CDW states. However, our analysis of the charge transfer as function of work function differences suggests this is a good approximation.

D. Charge transfer

Charge transfer is the central result of this work. To calculate the charge transfer between the different constituents of a heterostructure we followed the method presented in Refs.^{34,57}. This method is based on computing the charge density of the full structure with respect to that of a hypothetical reference structure built from the calculated charge densities of the isolated constituents, positioned in the places they would occupy in the full structure. More explicitly, if we consider \hat{z} as the stacking direction, we can obtain the plane-averaged charge density from the self-consistent calculations $\rho_{\text{all}}(z)$ and $\rho_i(z)$ with $i = 1, 2, \dots, N$, where N is the number of component, and obtain the overall charge density difference as

$$\rho_{\text{dif}}(z) = \rho_{\text{all}}(z) - \sum_{i=1}^N \rho_i(z), \quad (2)$$

Integrating $\rho_{\text{dif}}(z)$ we can obtain the total charge difference in a section (z_1, z_2) as

$$q_{\text{dif}}(z_1, z_2) = \int_{z_1}^{z_2} \rho_{\text{dif}}(z) dz. \quad (3)$$

Determining appropriate values for z_1 and z_2 can be challenging when $N > 2$ or for periodic systems, such as the 4H_b structure. A practical approach is to set z_1 as the point where $\rho_{\text{dif}}(z_1) = 0$ nearest to the interface

| | NbSe ₂ | NbS ₂ | TaSe ₂ | TaS ₂ |
|-------------------|-------------------|------------------|-------------------|------------------|
| $ \vec{u}_A $ (Å) | 0.00 | 0.00 | 0.00 | 0.00 |
| $ \vec{u}_B $ (Å) | 0.26 | 0.21 | 0.26 | 0.20 |
| $ \vec{u}_C $ (Å) | 0.32 | 0.28 | 0.31 | 0.25 |
| d (Å) | 7.37 | 6.89 | 7.51 | 7.10 |
| W_T (eV) | 5.25 | 5.47 | 5.02 | 5.19 |
| W_H (eV) | 5.57 | 6.13 | 5.45 | 5.57 |
| ΔWF (eV) | 0.32 | 0.66 | 0.43 | 0.77 |
| CT (e) | 0.12 | 0.23 | 0.14 | 0.26 |

TABLE I. Displacements for each inequivalent metallic position \vec{u}_i with $i = A, B, C$, interlayer distance d , work functions W_T and W_H for T and H structures, workfunction differences ΔWF and charge transfer CT for all four compounds considered.

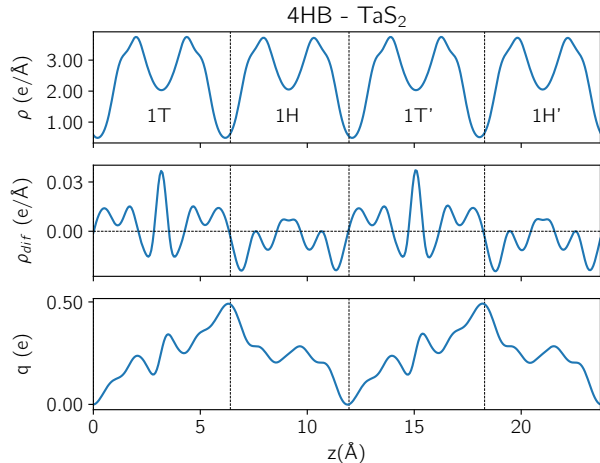


FIG. 2. Electronic density (top), electronic density difference (mid) and total charge change (bottom) for 4H_b TaS₂. Zeros for electronic density difference and thus candidates for z_1/z_2 are marked with vertical dashed lines.

with the preceding component, and z_2 as the point where $\rho_{\text{dif}}(z_2) = 0$ nearest to the interface with the subsequent component. For instance, in Fig. 2, the total charge difference for the T layer in 4H_b is obtained by integrating from $z_1 = 0$ Å to $z_2 = 6.40$ Å (where the vertical and horizontal dashed lines first intersect in the second graph); for H, integration ranges from $z'_1 = z_2 = 6.40$ Å to $z'_2 = 11.95$ Å, and so forth. These integration limits correspond to the maximum and minimum values of $q(0, z)$ as illustrated in the third graph. In the scenario of $N = 2$ isolated components, integration simplifies: as depicted in Fig. 3, z_1 may be positioned anywhere in vacuum, while $z_2 = 2$ marks the point where $\rho_{\text{dif}}(z_2) = 0$ nearest to the interface. $q(z_1, z_2)$ represents the total charge difference for the first component and the overall absolute charge transfer between components.

In Table I we present the charge transfer results for the relaxed interlayer distances. These distances are 6.89 Å for NbS₂, 7.37 Å for NbSe₂, 7.10 Å for TaS₂ and 7.51 Å for TaSe₂. Those values are plotted in Fig. 4, where the previously mentioned $CT \propto \Delta WF$ trend is clear. From these results, we can detect some trends: *ab-initio* calculations predict Ta compounds to have greater charge trans-

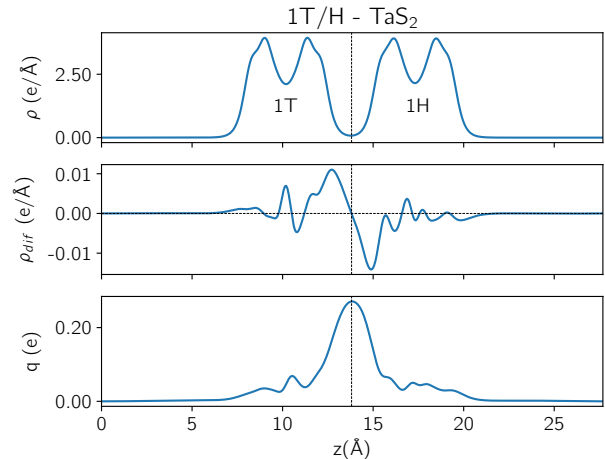


FIG. 3. Electronic density (top), electronic density difference (mid) and total charge change (bottom) for 1T/H TaS₂ bilayer. The zero for electronic density difference is marked with a vertical dashed line.

fer than Nb compounds, and S compounds have greater charge transfer than Se compounds.

E. Van der Waals effect

In this section, we compare the calculation of the charge transfer with and without Van der Waals corrections for the T/H structures obtained in Sec. IID. To do so we incorporated Van der Waals corrections into the electronic self-consistent calculations and repeated the charge transfer calculations in Sec. IID. Our findings indicate that these corrections have a negligible influence on charge transfer, typically on the order of $< 10^{-3}$.

While Van der Waals corrections therefore do not affect charge transfer directly, they could do so indirectly if we performed a new relaxation of the structure in the presence of such corrections, since the interlayer distance could change upon relaxation. Since our main interest in this work is to establish relative trends in charge transfer, we have rather opted to study charge transfer as a function of interlayer distance without attempting to calculate precisely its equilibrium value, as this is a more

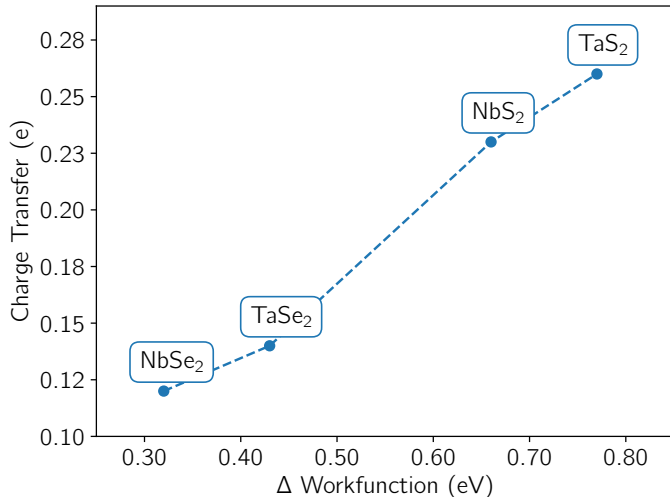


FIG. 4. Charge transfer as a function of workfunction difference between layers in 1T/H bilayer.

complex problem that depends on both calculational details and experimental conditions.

F. U dependence

Following the same logic as in the previous section, we now consider the effect of the Hubbard interaction U , only at the level of electronic self-consistent calculations keeping the structure fixed. We considered only TaS₂ as an example. The main effect of the Hubbard interaction is to magnetize the flat band near the Fermi level, producing a spin splitting and pushing one of the spin polarizations above the Fermi level. Since a larger magnetization is produced when the lower spin-split band is closer to half-filling, increasing U generally leads to a reduction in charge transfer to gain energy from magnetization. The effect should thus be larger in the compound with larger charge transfer, which is TaS₂. Figure 5 illustrates both charge transfer and magnetization of the center of the SoD as a function of U for this compound. As expected, charge transfer exhibits an inverse relationship with U , albeit the overall impact of U on charge transfer remains relatively minor (on the order of $10^{-2}e$). The critical U for the flat band magnetization is around $U_c \sim 1$ eV, as we can see from the spin split bands in Fig. B, where we also include a brief comment on the effect of U to the electronic band structures. The conclusion of this section is that while U might have a sizable effect in the bands and magnetization, is not so relevant for charge transfer.

G. Distance dependence

In order to explore the impact of interlayer distance on charge transfer, we calculated the charge transfer across

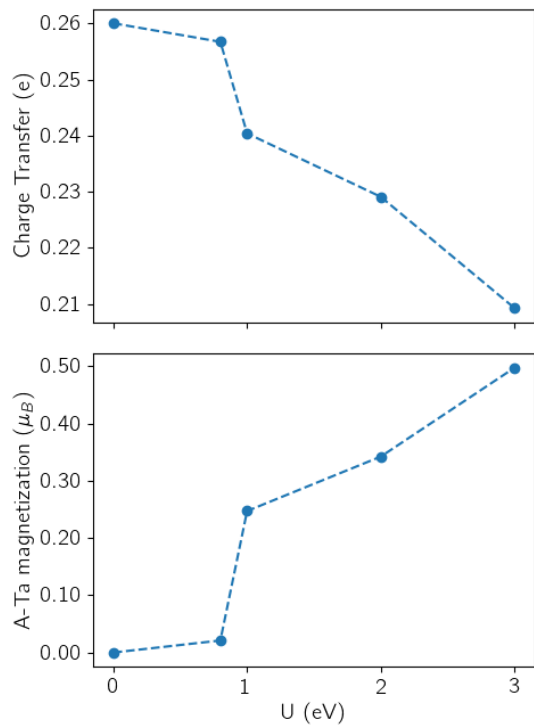


FIG. 5. Charge transfer (top) and magnetization of A atoms in the T layer (bottom) dependence on U for TaS₂.

a range of distances for experimentally reported compounds, encompassing both the relaxed values and those derived from experimental data. The structure of each layer, obtained after relaxation, is kept fixed as the interlayer distance is varied, as we expected the effect of further relaxation to be minimal except perhaps at very close distances. Experimental values were determined based on the reported interlayer spacings in bulk 4H_b materials. Specifically, for TaS₂ ($c = 23.73\text{\AA}$)²², the Ta-Ta interlayer distance is 5.93 Å. Likewise, for TaSe₂ ($c = 25.16\text{\AA}$)⁵⁸, the corresponding interlayer distance is 6.29 Å. For NbSe₂, the 4H_b polytype has not been reported, so we extrapolate its interlayer distance by comparison with TaSe₂. The interlayer distance in 2H-TaSe₂ is 6.35 Å, which is 1% less than that of 4H_b-TaSe₂¹. For 2H-NbSe₂ the interlayer distance is 6.27 Å, so assuming the same trend we can take 1% less for a hypothetical 4H_b-NbSe₂ structure, i.e. 6.21. NbS₂ was not included in this analysis due to lack of experimental data. It should be noted that the experimental interlayer distances in bulk compounds need not be the same as for bilayers on a substrate, so these values should be taken only as reference. In general, we also see that these values are smaller than those obtained from relaxation in Table I.

Figure 6 illustrates the interlayer distance dependence of charge transfer for NbSe₂, TaS₂, and TaSe₂. All three compounds exhibit a comparable trend in charge transfer as a function of distance, characterized by two distinct patterns: at larger interlayer distances, a gradual linear

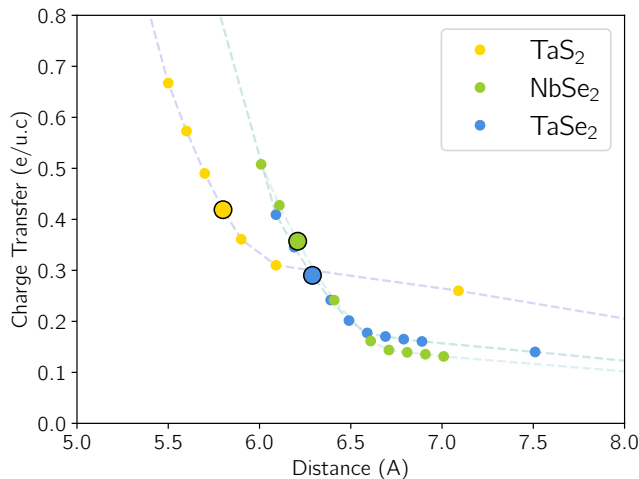


FIG. 6. Charge transfer dependence on interlayer distance for T/H bilayers of NbSe₂, TaS₂ and TaSe₂ in the non-magnetic state at $U = 0$. Experimental equilibrium distances for 4H_b compounds marked by a bigger dot with a black contour (for NbSe₂ an extrapolated value is used, see text).

increase in charge transfer is observed, while at smaller distances, a tipping point is reached, beyond which the rate of linear growth becomes more pronounced. From distances of 5.5 Å and below, our charge transfer calculation method becomes less reliable due to the ambiguity in defining the boundaries between subsystems in the presence of strong hybridization. We also observe that TaS₂ has the largest charge transfer also at the experimental interlayer distance.

In order to contextualize our findings within existing literature, we can now compare them by extrapolating to various distances. For instance, the results reported in Ref.¹⁰ predict a charge transfer of 0.32 e for TaSe₂ at an interlayer distance of 6.60 Å, which exceeds our result of around 0.20 e . Conversely, the investigation conducted on NbSe₂ in Ref.³⁵, where the interlayer distance is 6.08 Å, indicates a charge transfer of 0.17 e , lower than our predicted value of 0.43 e . Ref.³⁰ undertakes a similar analysis for TaS₂ but predicts higher overall charge transfers and a smoother evolution towards CT=1 at small distances, rather than the two-step dependence observed in our results. This disparity may arise from differences in the methods used for calculating charge transfer as well as in the relaxation procedure, since Ref.³⁰ performs a relaxation for each distance, which becomes progressively more important as interlayer hybridization increases. Our work is however generally consistent with the fact that interlayer distance is the key parameter that most strongly affects charge transfer, as put forward in Ref.³⁰.

III. RESULTS: BULK 4H_b POLYTOPES

To compare with the results obtained from bilayers, we calculated the charge transfer in 4H_b-TaS₂ and 4H_b-TaSe₂. We constructed the lattice structure in the CDW state by stacking the relaxed structures obtained from single layers in Sec. II A using experimentally reported interlayer distances.

The charge transfer results for 4H_b structures of TaS₂ and TaSe₂ compounds are 0.49 e/u.c. and 0.39 e/u.c., respectively. These outcomes exhibit consistency with those reported for bilayers and their distance dependence in the preceding sections. To understand these results we also computed the band structure projected to the A atom of the SoD in Fig. 7, as well as the partial DOS calculations for A,B and C atoms in Fig. 8, for the 4H_b structures of both compounds. Interestingly, TaS₂ displays a flat band which is nearly everywhere above the Fermi level, consistent with a peak in the DOS for the A atom in the range 0-0.4 eV. Taken at face value this figure would suggest a charge transfer of nearly 1 e/u.c. Similarly, in TaSe₂, the flat bands begin at $E \approx 0.3$ eV and $E \approx -0.2$ eV, with the latter seeming to hybridize and reach $E \approx 0.1$ eV after Γ , where it exhibits a higher DOS, as illustrated in Fig. 8. Charge transfer is harder to quantify in this case but it also appears larger than the computed value of 0.39. These disparities lead us to consider two potential explanations: firstly, that the behaviour of bands away from the high-symmetry k -path has a significant influence on charge transfer, as there might be bands with significant weight in the A atom below the Fermi level we simply do not see in the high symmetry path. Alternatively, interlayer hybridization might already be strong enough that charge transfer cannot be inferred directly from the population of the projected bands, and the computed numerical values should be taken as the reliable ones.

IV. CONCLUSION

In this work, we conduct detailed *ab-initio* study of charge transfer in 1T/H bilayers of MX₂ and 4H_b TaX₂ structures (M=Nb,Ta, X=S, Se), revealing its dependence on Hubbard U , Van der Waals corrections and interlayer distance. The most significant findings are summarized in Table I and illustrated in Fig. 6. Our results indicate that both U and Van der Waals corrections have minimal impact on charge transfer, despite a finite magnetization. In line with previous work for TaS₂³⁰, we find the interlayer distance to be the parameter on which charge transfer is most strongly dependent.

The main result of our work is to reveal the different trends across T/H compounds. Generally, X=Se compounds exhibit higher charge transfer compared to those with X=S, while M=Ta compounds also demonstrate greater charge transfer compared to M=Nb counterparts. Additionally, our method predicts charge transfer to be

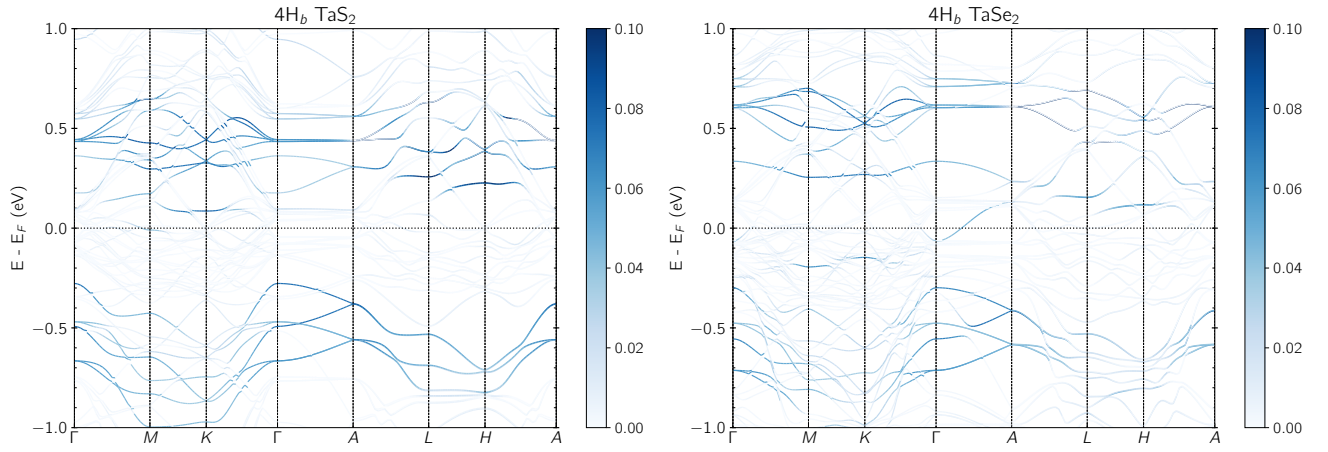


FIG. 7. Band structures for $4H_b$ -TaS₂ (left) and $4H_b$ -TaSe₂ (right) in the structure when the 1T layer is in the CDW state, color coded by the weight of the wave function in the central SoD atom A. The SoD centers for both T layers are on top of each other.

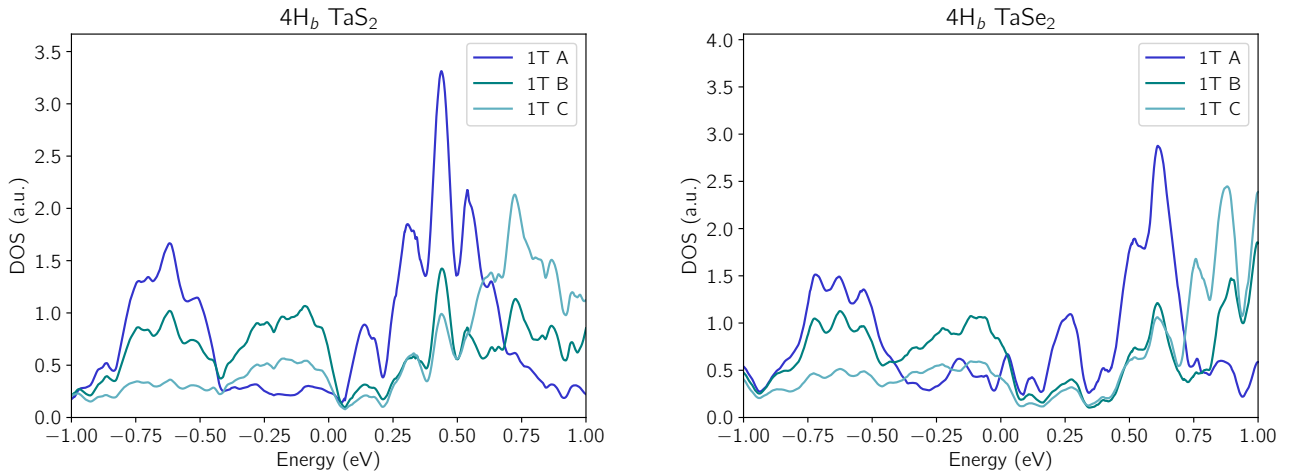


FIG. 8. A,B and C atom-projected DOS for 1T-TaS₂ (left) and 1T-TaSe₂ (right) in the $4H_b$ structure when the 1T layer is in the CDW state.

more pronounced in bulk $4H_b$ structures when compared to bilayers. These findings may have important experimental implications. First, there are clear differences in the behaviour of the Kondo peak in T/H bilayers in TaSe₂^{9,10}, TaS₂^{11,12} and NbSe₂^{13,14}, as well as in the orbital character of the higher energy states⁹. Rather than inconsistencies between experiments, these features may reveal that charge transfer and the proximity to the potential Mott insulator state may be different across compounds, and more work is needed to determine charge transfer for each of them experimentally. Similarly, $4H_b$ TaS₂ appears to have larger CT with more clear evidence of nearly unoccupied flat band^{19,20,24} which plays a minor role in superconductivity, but our calculations suggest the flat band might be more populated in $4H_b$ TaSe₂ and have a stronger effect on the superconducting state⁵⁹⁻⁶¹. We hope that our results will stimulate

further work to experimentally map out charge transfer across the family of T/H structures, which will lead to a deeper understanding of the unconventional magnetic and superconducting properties in this family of materials.

V. ACKNOWLEDGEMENTS

We acknowledge useful discussions with M. Ugeda and M. Gastiasoro. F. J. is supported by Grant PID2021-128760NB0-I00 from the Spanish MCIN/AEI/10.13039/501100011033/FEDER, EU. M.G.V. and I.S. thank support from the Deutsche Forschungsgemeinschaft (DFG, German Research Foundation) GA3314/1-1 -FOR 5249 (QUAST) and to the Spanish Ministerio de Ciencia e Innovacion grant

PID2022-142008NB-I0. M.G.V. acknowledges partial support from the European Research Council (ERC) under grant agreement no. 101020833.

POSCARS used and obtained are present in supplementary files.

Appendix A: Displacements

We present the positions for CDW and no CDW configurations along the displacements for all four TMDs in Fig. 9. All relaxed CDW systems were obtained from a calculation whose initial state had small displacements following the trend of our previous work¹⁰. All VASP's

Appendix B: U bands

In this section, we include the spin-projected electronic bandstructures from TaS₂ bilayer for all four U different values, see Fig. 10. We can determine that the overall effect of U is to split the T flat band, pushing the spin up band below the Fermi energy and the spin down one up into valence bands, thus increasing magnetization of this band and a hindering of the charge transfer.

- ¹ V. Kalikhman and Y. S. Umanskiĭ, Soviet Physics Uspekhi **15**, 728 (1973).
- ² J. A. Wilson, F. Di Salvo, and S. Mahajan, Advances in Physics **24**, 117 (1975).
- ³ K. Rossnagel, Journal of Physics: Condensed Matter **23**, 213001 (2011).
- ⁴ As it is often done, we label the two-dimensional polytypes with letters T and H, and the bulk polytypes as 1T, 2H, 4H_b... , where the number refers to the number of layers in the unit cell.
- ⁵ P. Fazekas and E. Tosatti, Physica B+ C **99**, 183 (1980).
- ⁶ K. Rossnagel and N. V. Smith, Phys. Rev. B **73**, 073106 (2006).
- ⁷ K. T. Law and P. A. Lee, Proceedings of the National Academy of Sciences **114**, 6996 (2017).
- ⁸ T. Ritschel, H. Berger, and J. Geck, Phys. Rev. B **98**, 195134 (2018).
- ⁹ W. Ruan, Y. Chen, S. Tang, J. Hwang, H.-Z. Tsai, R. L. Lee, M. Wu, H. Ryu, S. Kahn, F. Liou, et al., Nature Physics **17**, 1154 (2021).
- ¹⁰ W. Wan, R. Harsh, A. Meninno, P. Dreher, S. Sajan, H. Guo, I. Errea, F. de Juan, and M. M. Ugeda, Nature Communications **14**, 7005 (2023).
- ¹¹ V. Vaño, M. Amini, S. C. Ganguli, G. Chen, J. L. Lado, S. Kezilebieke, and P. Liljeroth, Nature **599**, 582 (2021).
- ¹² C. G. Ayani, M. Pisarra, I. M. Ibarburu, M. Garnica, R. Miranda, F. Calleja, F. Martín, and A. L. Vázquez de Parga, Small **23**, 2303275 (2023).
- ¹³ M. Liu, J. Leveillee, S. Lu, J. Yu, H. Kim, C. Tian, Y. Shi, K. Lai, C. Zhang, F. Giustino, et al., Science advances **7**, eabi6339 (2021).
- ¹⁴ S. C. Ganguli, J. L. Lado, and P. Liljeroth, arXiv:2401.08296 (2024).
- ¹⁵ F. Di Salvo, B. Bagley, J. Voorhoeve, and J. Waszczak, Journal of Physics and Chemistry of Solids **34**, 1357 (1973).
- ¹⁶ F. J. Di Salvo, D. E. Moncton, J. A. Wilson, and S. Mahajan, Phys. Rev. B **14**, 1543 (1976).
- ¹⁷ A. Achari, J. Bekaert, V. Sreepal, A. Orekhov, P. Kumaravadivel, M. Kim, N. Gauquelin, P. Balakrishna Pillai, J. Verbeeck, F. M. Peeters, et al., Nano Letters **22**, 6268 (2022).
- ¹⁸ S. Pal, P. Bahera, S. Sahu, H. Srivastava, A. Srivastava, N. Lalla, R. Sankar, A. Banerjee, and S. Roy, Physica B: Condensed Matter **669**, 415266 (2023).
- ¹⁹ S. Shen, T. Qin, J. Gao, C. Wen, J. Wang, W. Wang, J. Li, X. Luo, W. Lu, Y. Sun, et al., Chinese Physics Letters **39**, 077401 (2022).
- ²⁰ A. K. Nayak, A. Steinbok, Y. Roet, J. Koo, I. Feldman, A. Almoalem, A. Kanigel, B. Yan, A. Rosch, N. Avraham, and H. Beidenkopf, PNAS **120**, e2304274120 (2023).
- ²¹ D. Dentelski, E. Day-Roberts, T. Birol, R. M. Fernandes, and J. Ruhman, Phys. Rev. B **103**, 224522 (2021).
- ²² A. Ribak, R. M. Skiff, M. Mograbi, P. Rout, M. Fischer, J. Ruhman, K. Chashka, Y. Dagan, and A. Kanigel, Science advances **6**, eaax9480 (2020).
- ²³ E. Persky, A. V. Bjørlig, I. Feldman, A. Almoalem, E. Altman, E. Berg, I. Kimchi, J. Ruhman, A. Kanigel, and B. Kalisky, Nature **607**, 692 (2022).
- ²⁴ A. K. Nayak, A. Steinbok, Y. Roet, J. Koo, G. Margalit, I. Feldman, A. Almoalem, A. Kanigel, G. A. Fiete, B. Yan, et al., Nature physics **17**, 1413 (2021).
- ²⁵ A. Almoalem, I. Feldman, M. Shlafman, Y. E. Yaish, M. H. Fischer, M. Moshe, J. Ruhman, and A. Kanigel, arXiv:2208.13798 (2022).
- ²⁶ I. Silber, S. Mathimalar, I. Mangel, A. Nayak, O. Green, N. Avraham, H. Beidenkopf, I. Feldman, A. Kanigel, A. Klein, et al., Nature Communications **15**, 824 (2024).
- ²⁷ R. Friend, R. Frindt, A. Grant, A. Yoffe, and D. Jerome, Journal of Physics C: Solid State Physics **10**, 1013 (1977).
- ²⁸ A. Beal, Journal of Physics C: Solid State Physics **11**, 4583 (1978).
- ²⁹ N. Doran, G. Wexler, and A. Woolley, Journal of Physics C: Solid State Physics **11**, 2967 (1978).
- ³⁰ L. Crippa, H. Bae, P. Wunderlich, I. I. Mazin, B. Yan, G. Sangiovanni, T. Wehling, and R. Valentí, Nature Communications **15**, 1357 (2024).
- ³¹ A. Almoalem, R. Gofman, Y. Nitzav, I. Mangel, I. Feldman, J. Koo, F. Mazzola, J. Fujii, I. Vobornik, J. Sánchez Barriga, et al., npj Quantum Materials **9**, 36 (2024).
- ³² J.-A. Yan, M. A. D. Cruz, B. Cook, and K. Varga, Scientific reports **5**, 16646 (2015).
- ³³ J. J. Gao, J. G. Si, X. Luo, J. Yan, Z. Z. Jiang, W. Wang, Y. Y. Han, P. Tong, W. H. Song, X. B. Zhu, Q. J. Li, W. J. Lu, and Y. P. Sun, Phys. Rev. B **102**, 075138 (2020).
- ³⁴ Z. Wang, Y.-Y. Sun, I. Abdelwahab, L. Cao, W. Yu, H. Ju, J. Zhu, W. Fu, L. Chu, H. Xu, et al., ACS nano **12**, 12619 (2018).
- ³⁵ R. Pico, P. Abufager, I. Hamad, R. Robles, and N. Lorente, arxiv:2403.03302 (2024).

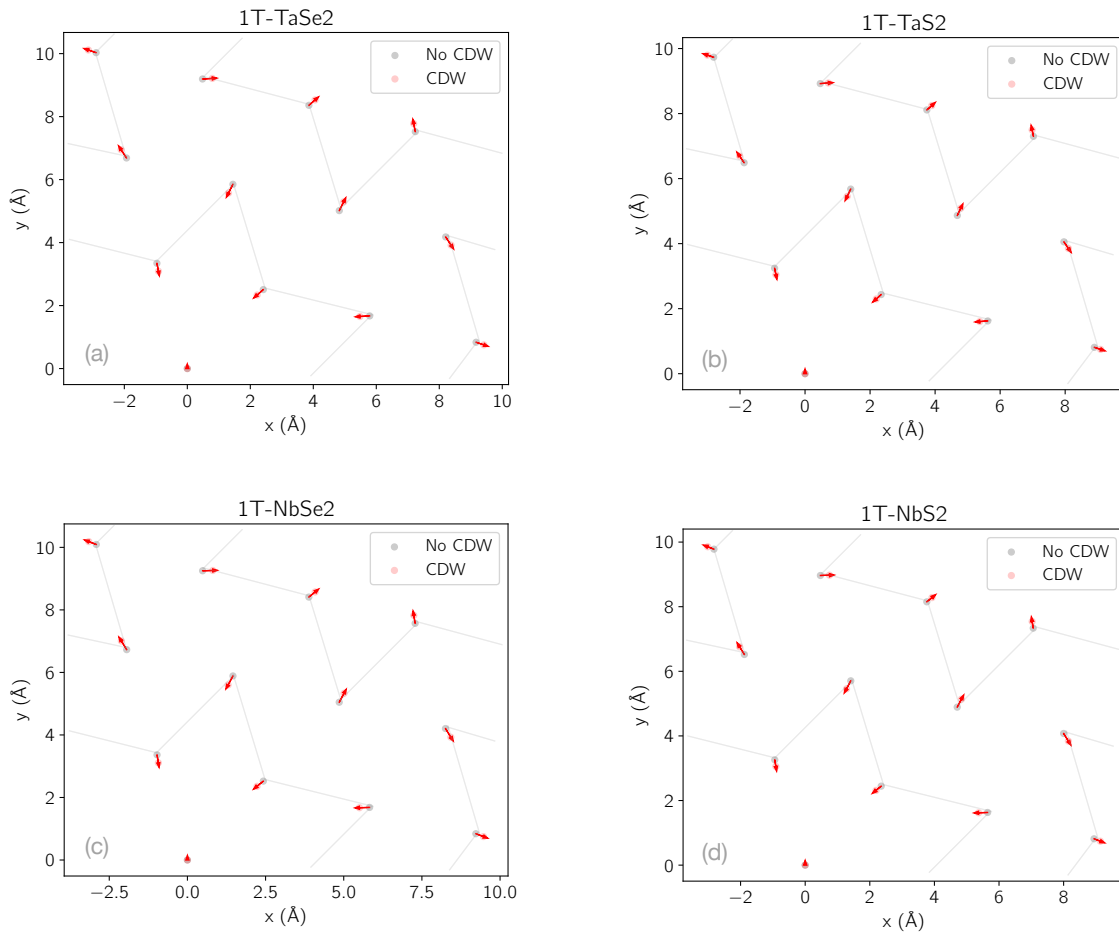


FIG. 9. CDW and no CDW atomic positions and displacements of (a) 1T-TaSe₂ (b) 1T-TaS₂ (c) NbSe₂ and (d) 1T-NbS₂. SoD CDW its superimposed in order to show the different symmetry positions A,B and C.

- ³⁶ P. Darancet, A. J. Millis, and C. A. Marianetti, *Phys. Rev. B* **90**, 045134 (2014).
- ³⁷ Q. Zhang, L.-Y. Gan, Y. Cheng, and U. Schwingenschlög, *Phys. Rev. B* **90**, 081103 (2014).
- ³⁸ X.-L. Yu, D.-Y. Liu, Y.-M. Quan, J. Wu, H.-Q. Lin, K. Chang, and L.-J. Zou, *Phys. Rev. B* **96**, 125138 (2017).
- ³⁹ S. Yi, Z. Zhang, and J.-H. Cho, *Phys. Rev. B* **97**, 041413 (2018).
- ⁴⁰ Y. Chen, W. Ruan, M. Wu, S. Tang, H. Ryu, H.-Z. Tsai, R. L. Lee, S. Kahn, F. Liou, C. Jia, et al., *Nature Physics* **16**, 218 (2020).
- ⁴¹ T. Jiang, T. Hu, G.-D. Zhao, Y. Li, S. Xu, C. Liu, Y. Cui, and W. Ren, *Phys. Rev. B* **104**, 075147 (2021).
- ⁴² J. W. Park and H. W. Yeom, arXiv:2008.05702 (2020).
- ⁴³ E. Kamil, J. Berges, G. Schönhoff, M. Rösner, M. Schüler, G. Sangiovanni, and T. Wehling, *J. Phys.: Cond. Matter* **30**, 325601 (2018).
- ⁴⁴ D. Pasquier and O. V. Yazyev, *Phys. Rev. B* **98**, 045114 (2018).
- ⁴⁵ C. Tresca and M. Calandra, *2D Materials* **6**, 035041 (2019).
- ⁴⁶ K. Zhang, C. Si, C.-S. Lian, J. Zhou, and Z. Sun, *J. Mater. Chem. C* **8**, 9742 (2020).
- ⁴⁷ D. Pasquier and O. V. Yazyev, arxiv:2108.11277.
- ⁴⁸ J. Zaanen, G. A. Sawatzky, and J. W. Allen, *Phys. Rev. Lett.* **55**, 418 (1985).
- ⁴⁹ J. Phillips, J. L. Lado, V. Pardo, and A. O. Fumega, arXiv:2306.12493 (2023).
- ⁵⁰ G. Kresse and J. Furthmüller, *Phys. Rev. B* **54**, 11169 (1996).
- ⁵¹ G. Kresse and J. Furthmüller, *Computational Materials Science* **6**, 15 (1996).
- ⁵² J. P. Perdew, K. Burke, and M. Ernzerhof, *Phys. Rev. Lett.* **77**, 3865 (1996).
- ⁵³ S. Grimme, J. Antony, S. Ehrlich, and H. Krieg, *The Journal of Chemical Physics* **132** (2010), 10.1063/1.3382344.
- ⁵⁴ S. L. Dudarev, G. A. Botton, S. Y. Savrasov, C. J. Humphreys, and A. P. Sutton, *Phys. Rev. B* **57**, 1505 (1998).
- ⁵⁵ M.-T. Huebsch, T. Nomoto, M.-T. Suzuki, and R. Arita, *Phys. Rev. X* **11**, 011031 (2021).
- ⁵⁶ U. Herath, P. Tavazze, X. He, E. Bousquet, S. Singh, F. Muñoz, and A. H. Romero, *Computer Physics Communications* **251**, 107080 (2020).
- ⁵⁷ X. Jiang, T. Yilmaz, E. Vescovo, and D. Lu, (2023), arXiv:2312.05112 [cond-mat.mtrl-sci].
- ⁵⁸ R. Morbt and E. Tronc, *Philosophical Magazine B* **40**, 305 (1979).

⁵⁹ Y. Liu, L. Li, W. Lu, R. Ang, X. Liu, and Y. Sun, *Journal of Applied Physics* **115** (2014).

⁶⁰ Z. Xie, M. Yang, Z. G. Cheng, T. Ying, J.-g. Guo, and X. Chen, *Journal of the Physical Society of Japan* **92**,

054702 (2023).

⁶¹ Q. Liu, P. Sun, F. Meng, Y. Geng, Z. Liu, J. Zhang, J. Gao, Z. Jiang, S. Tian, X. Luo, Y. Sun, Z. Cheng, K. Liu, H. Lei, and S. Wang, *Phys. Rev. B* **108**, 115115 (2023).

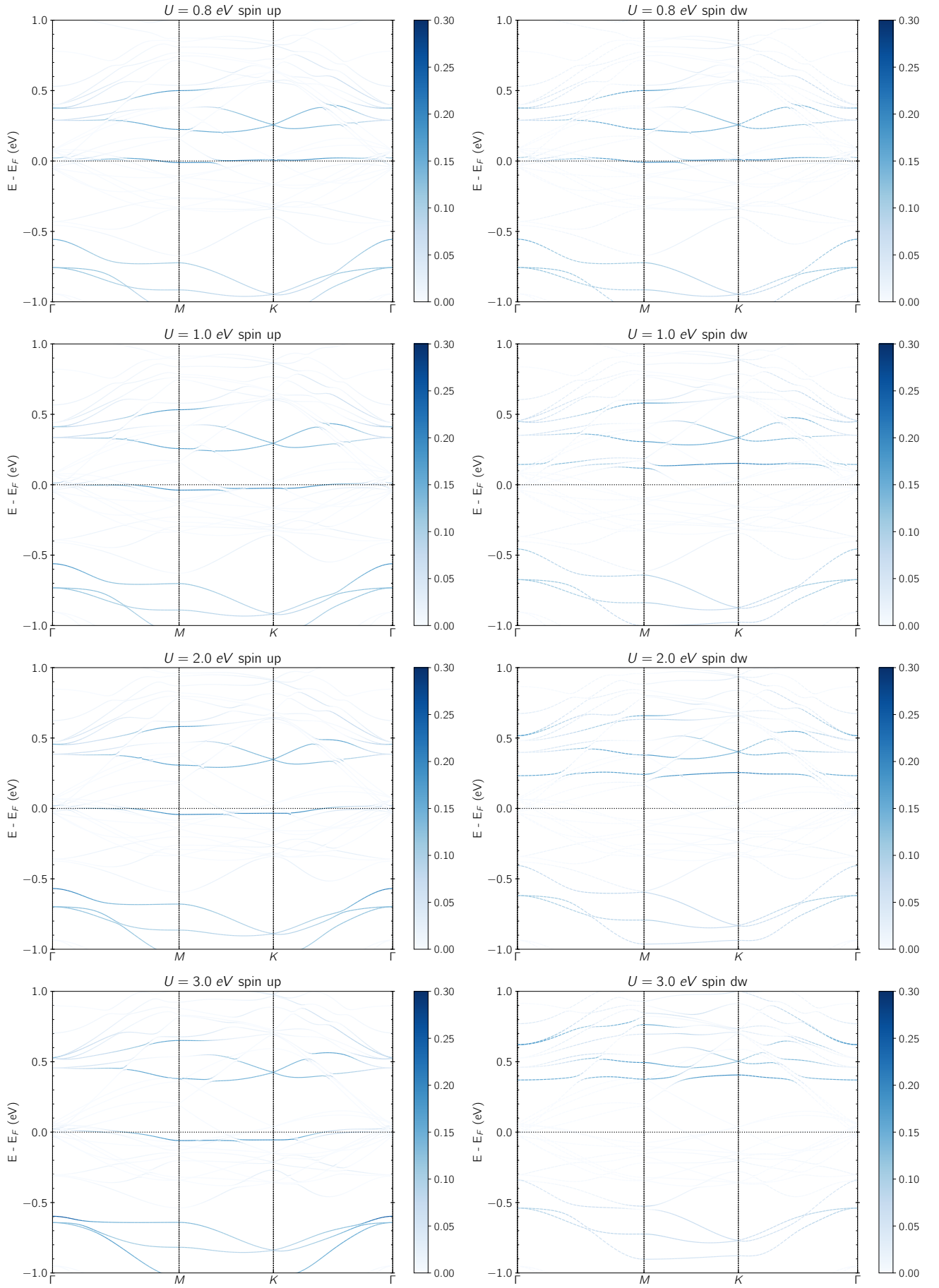


FIG. 10. T-H TaS₂ electronic atom-projected (T A atom) bandstructures for the different values for U considered in the main text and both spin polarizations.